Magnetic field amplification and particle acceleration in young SNRs

V.N.Zirakashvili

Pushkov Institute for Terrestrial Magnetism, Ionosphere and Radiowave Propagation, Russian Academy of Sciences (IZMIRAN), 142190 Troitsk, Moscow Region, Russia

Diffusive Shock Acceleration

Krymsky 1977; Bell 1978

Very attractive feature: power-law spectrum of particles accelerated, $\gamma=(\sigma+2)/(\sigma-1)$, where σ is the shock compression ratio, for strong shocks $\sigma=4$ and $\gamma=2$

Maximum energy for SN: $D\sim 0.1 u_{sh} R_{sh}$

$\sim 3\cdot 10^{27}$ cm^2/s$< D_{gal}$

Diffusion coefficient should be small in the vicinity of SN shock

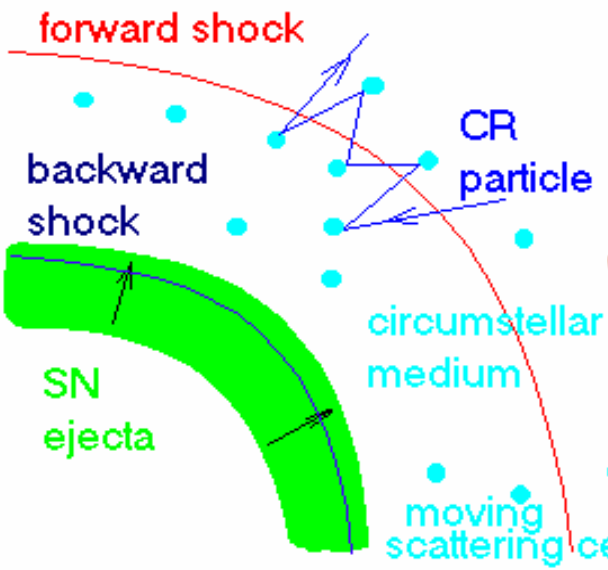

In the Bohm limit $D=D_B=cr_g/3$ and for interstellar magnetic field

$$E_{\max} = Z\cdot 10^{14}\,\mathrm{eV}\left(\frac{B}{10\,\mu\mathrm{G}}\right)\left(\frac{R_{\mathrm{sh}}}{3\,\mathrm{pc}}\right)\left(\frac{u_{\mathrm{sh}}}{3000\ \mathrm{km\ s^{-1}}}\right)$$

Cosmic ray streaming instability

Lerche 1967, Wentzel, 1969

$$\omega - k v_z = \pm \Omega ,$$

$$\Gamma(k) \approx \Omega_i \frac{N_{CR}(r_g > k^{-1})}{n_{pl}} \left(\frac{u_{CR}}{v_a} - 1 \right)$$

CR streaming amplifies MHD waves. CR particles are scattered by these waves (Bell, 1978). $k^{-1} \sim r_g$

$$\frac{\partial E_W}{\partial t} = \left| V_A \nabla P_{CR} \right|$$

without damping of MHD waves

Caprioli et al. 2009

$$\frac{\partial E_g}{\partial t} = \left| V_A \nabla P_{CR} \right|$$

strong damping of MHD waves

Heating of upstream plasma, Völk and McKenzie, 1981

Magnetic field amplification is necessary for acceleration of CR protons up to the knee energy $3 \cdot 10^{15}$ eV

$$u \frac{\partial}{\partial x} \frac{\langle \delta B^2 \rangle}{4\pi} = V_A \frac{\partial}{\partial x} P_{CR}$$

without wave damping

For modified shock

$$P_{CR} = \xi_{CR} \rho u^2, \quad \xi_{CR} \approx 0.5$$

$$\frac{\langle \delta B^2 \rangle}{B_0^2} = \xi_{CR} \frac{u}{V_A}$$

Shows the possibility to amplify MHD waves up to values δB/B~1. At higher amplitudes the quasilinear theory is not applicable. The Bohm diffusion is well justified.

Magnetic field amplification by non-resonant streaming instability

Bell (2004) used Achterberg's results (1983) and found the regime of instability that was overlooked

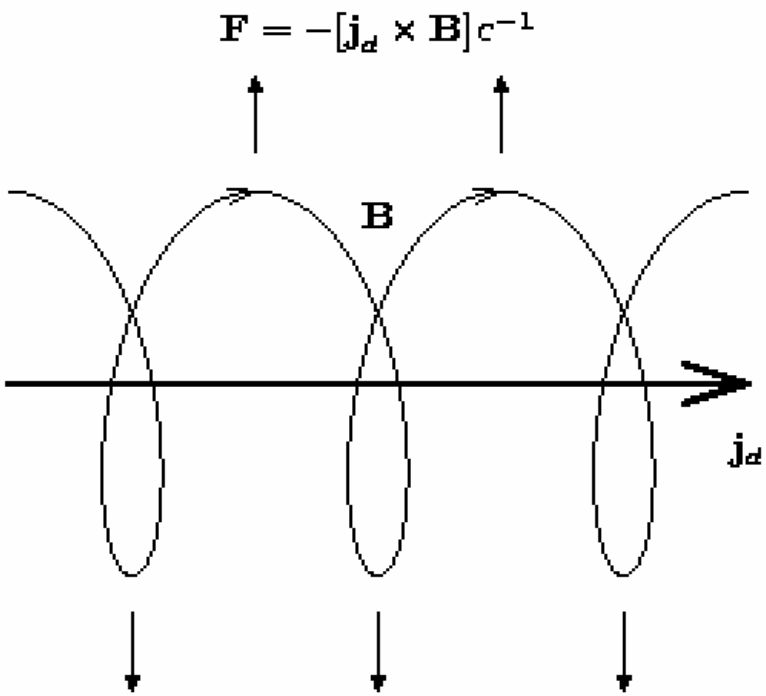

$$F_{CR} = -\frac{1}{c}\left[j_d \times B\right]$$

$$\omega^2 = V_a^2 k^2 - j_d \frac{B_0 k}{c\rho_0}$$

$$k\, r_g >> 1,\ \gamma_{max} = j_d B_0 / 2c\rho V_a$$

Since the CR trajectories are weakly influenced by the small-scale field, the use of the mean j_d is well justfied

saturated level of instability

$$B \approx \frac{4\pi}{ck} j_d$$

MHD modeling of non-resonant instability

Zirakashvili et al. 2008

J=16 3D 256^3

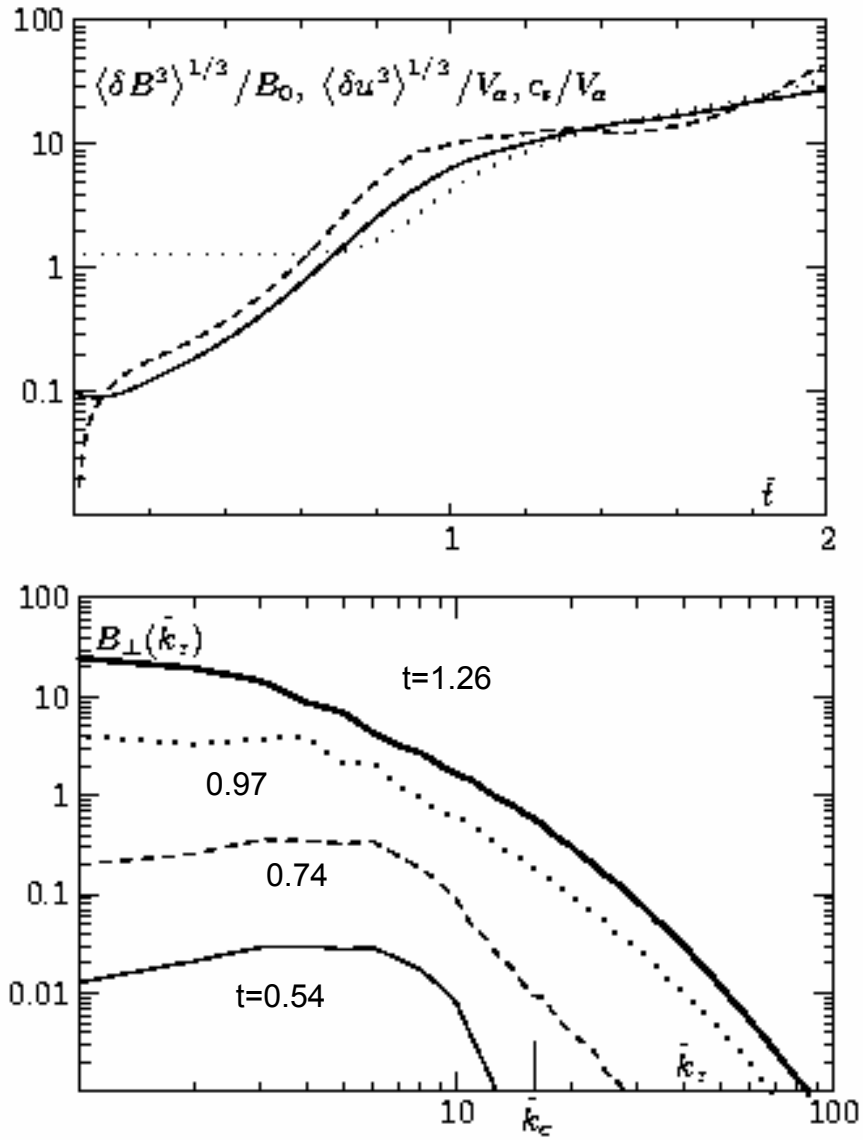

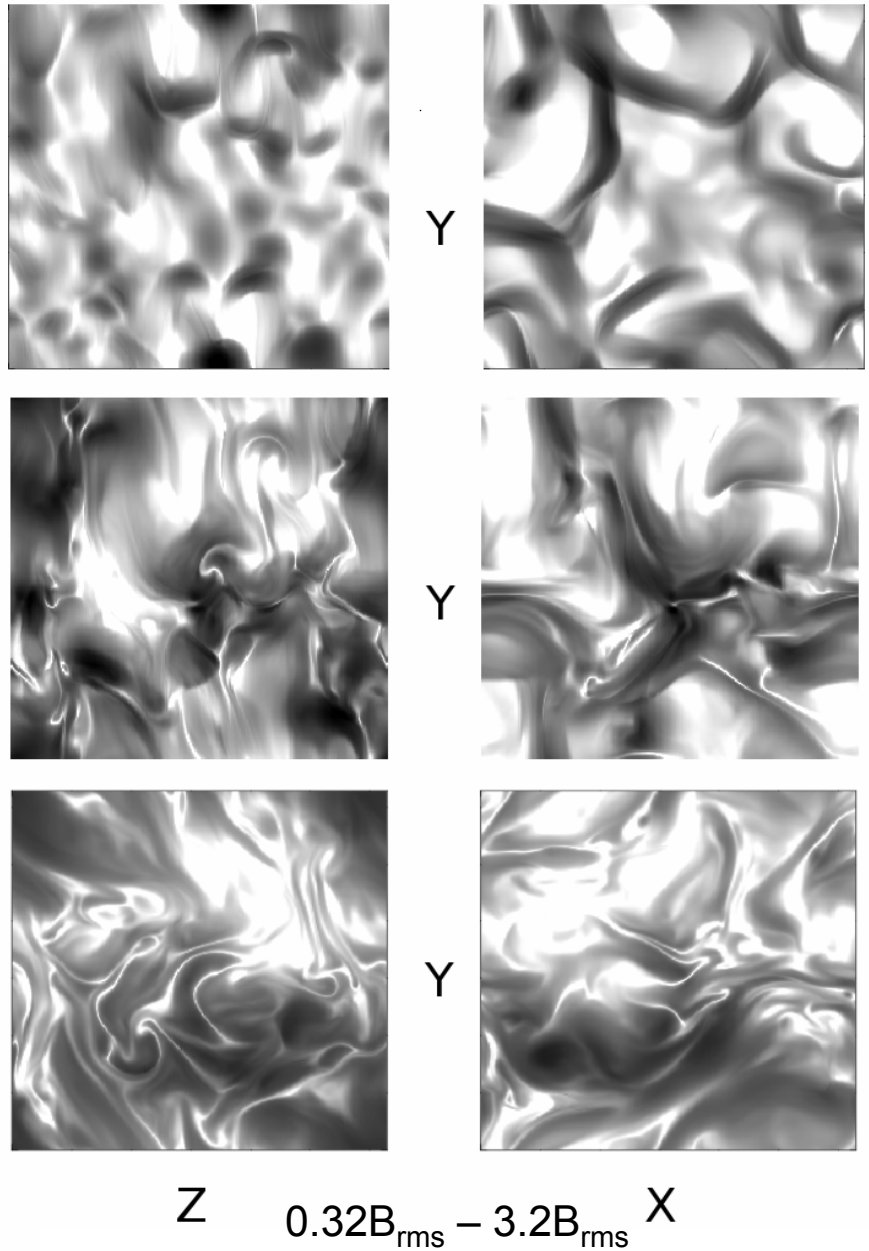

CR acceleration and magnetic amplification at the plane parallel steady shock

Zirakashvili & Ptuskin 2008

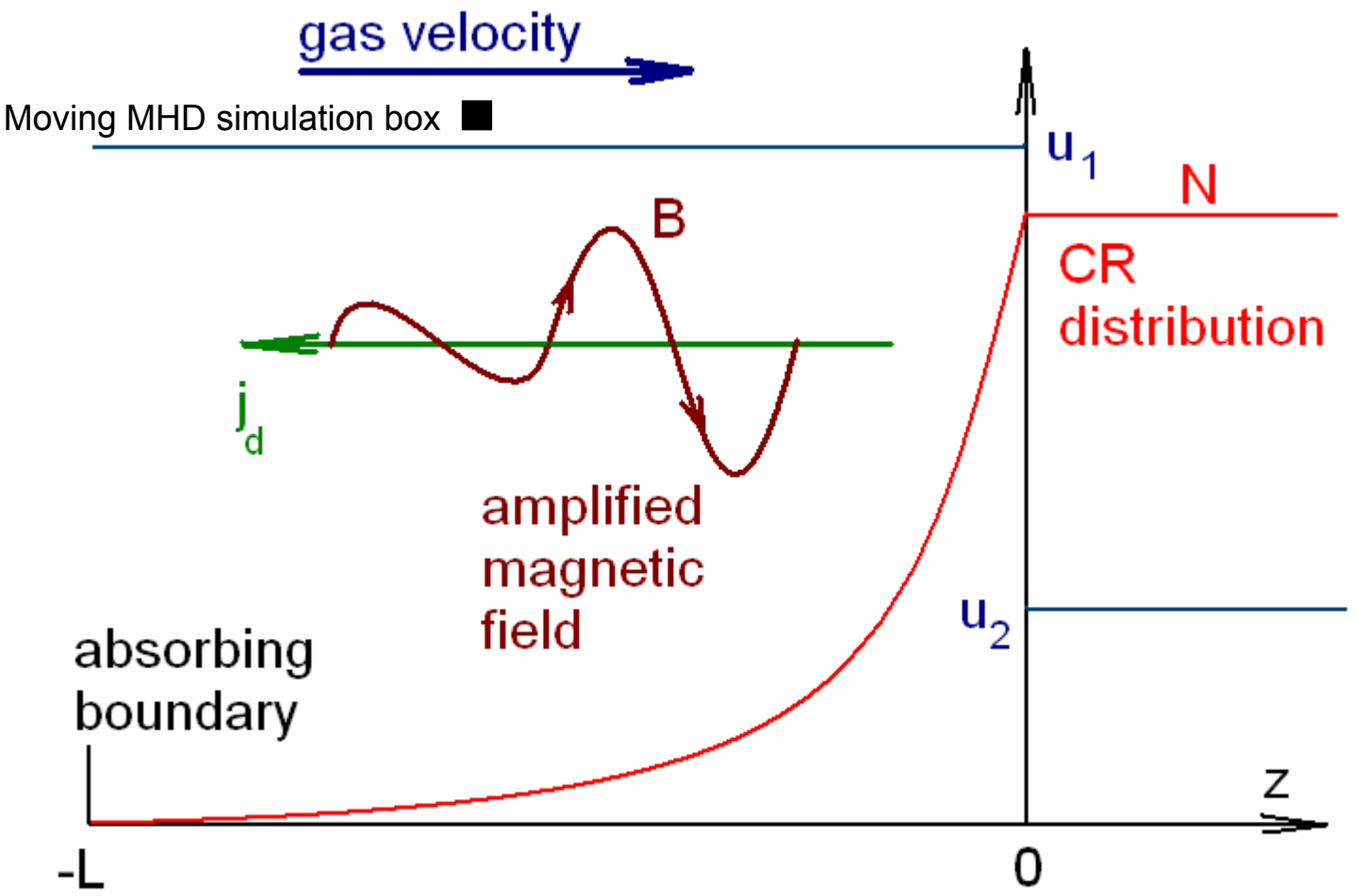

Background random magnetic field is prescribed at absorbing boundary

Cosmic ray transport equation

$$\frac{\partial N}{\partial t} = \nabla D \nabla N - \mathbf{u}\nabla N + \frac{p}{3}\frac{\partial N}{\partial p}\nabla \mathbf{u}$$

Krymsky 1964, Parker 1965, Dolginov & Toptygin 1966

$$N(z,p) = N_0(p)\frac{1-\exp\int_{-L}^{z} u dz'/D(z',p)}{1-\exp\int_{-L}^{0} u dz'/D(z',p)}$$

$$u\frac{p}{\gamma_s}\frac{\partial N_0}{\partial p} = D\frac{\partial N}{\partial z}\bigg|_{z=+0} - D\frac{\partial N}{\partial z}\bigg|_{z=-0}, \quad \gamma_s = \frac{3\sigma}{\sigma-1}$$

$$p\frac{\partial N_0}{\partial p} = -\frac{\gamma_s N_0}{1-\exp\left(-\int_{-L}^{0} u dz/D(z,p)\right)}$$

Dolginov-Toptygin (1967) small-scale approximation $kr_g >> 1$

Particles move along almost strait trajectories through the random magnetic inhomogeneities. Justified even for zero mean field.

$$\frac{\partial f_0}{\partial t} + \mathbf{v}\nabla f_0 + q\left(\mathbf{E}_0 + \frac{1}{c}[(\mathbf{v}-\mathbf{u}_0)\times\mathbf{B}_0]\right)\frac{\partial f_0}{\partial \mathbf{p}} = \frac{\partial}{\partial p_i}\nu_{ij}\frac{\partial f_0}{\partial p_j} \qquad (8)$$

Here $\mathbf{E}_0 = -c^{-1} < \delta\mathbf{u}\times\delta\mathbf{B} >$ is the mean electric field in the frame of reference moving with the mean plasma velocity $\mathbf{u}_0$.

The scattering tensor in the last equation ν_{ij} is determined by the spectrum of the random magnetic field $B_{ij}(\mathbf{k}) = \int \frac{d^3r}{(2\pi)^3} < B_i(\mathbf{r}+\mathbf{r}_0)B_j(\mathbf{r}_0) > \exp(-i\mathbf{kr})$:

$$\nu_{ij} = \frac{q^2}{c^2}\pi\int d^3k\,\delta(\mathbf{k}(\mathbf{v}-\mathbf{u}_0))\,e_{ilm}e_{jrs} \times B_{lr}(\mathbf{k})(v_m - u_{0m})(v_s - u_{0s}) \qquad (9)$$

Here e_{ijk} is the antisymmetric tensor. The scattering tensor makes the cosmic ray distribution isotropic in the frame moving with the velocity $\mathbf{u}_0$. The expression (9) may be simplified in the case of an isotropic random magnetic field $B_{ij}(\mathbf{k}) = \frac{1}{2}B_{isotr}(k)(\delta_{ij} - k_ik_j/k^2)$ (Dolginov & Toptygin (1967)):

$$\nu_{ij} = p^2\nu(p)\frac{(\mathbf{v}-\mathbf{u}_0)^2\delta_{ij} - (v_i - u_{0i})(v_j - u_{0j})}{2v|\mathbf{v}-\mathbf{u}_0|} \qquad (10)$$

where the scattering frequency $\nu(p)$ is given by the formula

$$\nu(p) = \frac{\pi}{4}\frac{q^2v}{p^2c^2}\int d^3k\,B_{isotr}(k)/k \qquad (11)$$

Here the spectrum of the isotropic magnetic field is normalized as $< \delta B^2 > = \int d^3k B_{isotr}(k)$.

Analytical solution for CR distribution

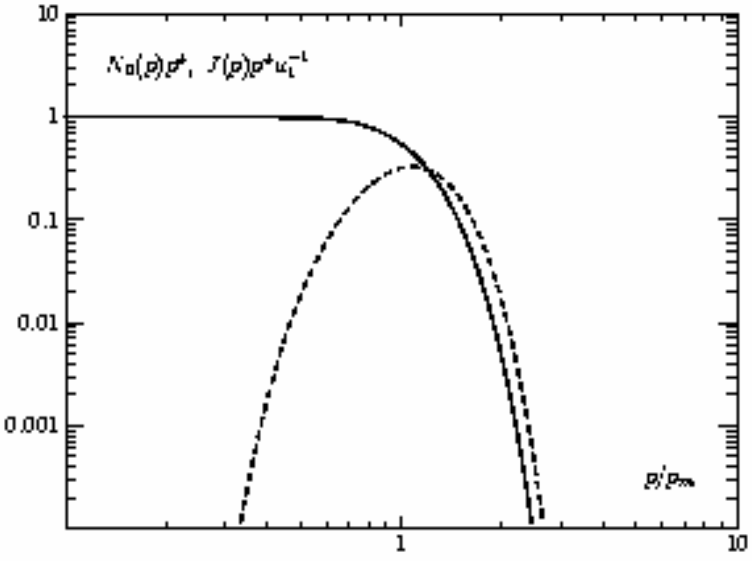

Fig. 1.— The momentum distribution at the shock $N_0(p)$ (solid line) and the cosmic ray flux $J(p)$ (dashed line) at the absorbing boundary at $z = -L$. The shock compression ratio is $\sigma = 4$.

$$p_m^3 = \frac{3\pi}{2}\frac{q^3 u_1}{c^3}\int_{-L}^{0} dz\, b(z) \qquad (20)$$

where the function $b(z)$ is given by the equation

$$b(z) = \left[\int^{\pi/2} \frac{(3/8)\sin^3\theta d\theta}{\int d^3k B_{xx}(k,z)\delta(k_z\cos\theta + k_x\sin\theta)}\right]^{-1}$$

$$j_d(z) = \frac{\eta_{cr}\rho u_1^3 q}{2cp_m I}\int_0^{\infty} ds\, s^{2-\gamma_s}\frac{\exp\left(\frac{a(z)}{p^2 a(0)}\right)}{\exp(s^{-2})-1} n_0(s), \qquad (24)$$

where $a(z) = \int_{-L}^{z} dz_1 b(z_1)$.

$$n_0(s) = \exp\left(-\gamma_s\int_0^{s}\frac{ds_1/s_1}{\exp(s_1^{-2})-1}\right).$$

We shall use the value $\gamma_s = 4$ and $I = 1/4$

$$N_0(p) = \frac{\eta_{cr}\rho u_1^2}{8\pi c p^{\gamma_s} p_m^{4-\gamma_s} I} n_0(p/p_m).$$

$\eta_{cr}=\eta_{esc}=2F_E/\rho u_1^3$ - CR energy flux at abs. boundary normalized to the kinetic energy flux

Modeling of the non-resonant instability with DSA

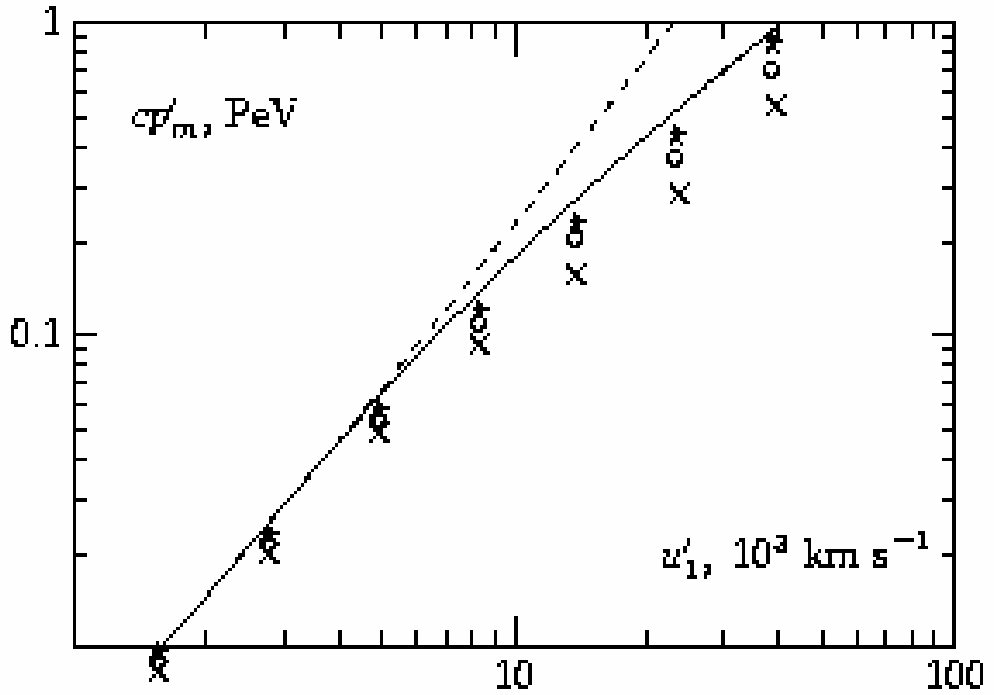

Fig. 5.— The dependence of the normalized maximum momentum p'_m on the normalized shock velocity u'_1. The results were obtained using the resolution 64^3 (crosses), 128^3 (open circles) and 256^3 (stars). The analytic approximation and the upper limit according to Eq. (40) are shown by the solid and dashed lines respectively.

$$j_d(\tilde{t}) = J_0 \int_0^\infty \frac{ds}{s^3} \frac{\exp\left(gs^{-3}\int_0^{\tilde{t}} d\tilde{t}'\, b(\tilde{t}')\right)}{\exp(s^{-3})-1} n_0(s)$$

Normalized shock velocity

$$u'_1 = u_1 \left(\frac{V_a}{10\ \mathrm{km\ s^{-1}}}\right)^{-3/4} \left(\frac{\eta_{cr}}{0.05}\right)^{1/3}$$

Normalized maximum momentum

$$p'_m = p_m \left(\frac{V_a}{10\ \mathrm{km\ s^{-1}}}\right)^{-1/3} \left(\frac{L}{1\ \mathrm{pc}}\right)^{-1} \left(\frac{B_0}{5\mu\mathrm{G}}\right)^{-1}$$

Non-resonant instability works for fast enough shocks

$$u_1 > (4cV_a^2/\eta_{cr})^{1/3}$$

$$= 1340\ \mathrm{km\ s^{-1}} \left(\frac{V_a}{10\ \mathrm{km\ s^{-1}}}\right)^{2/3} \left(\frac{\eta_{cr}}{0.05}\right)^{-1/3}$$

Summary of numerical results

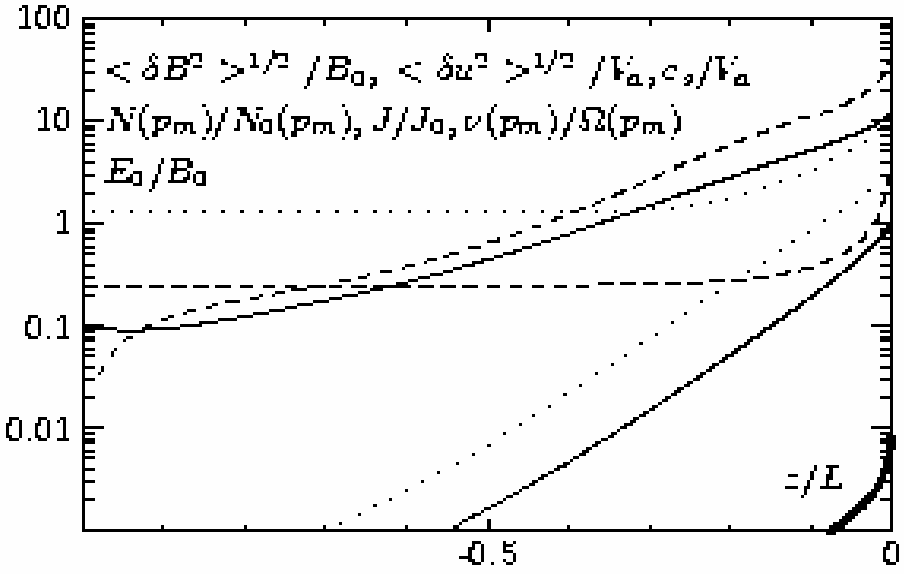

Fig. 6.— The dependence of the random magnetic field (solid line), turbulent velocity (dashed line), sonic velocity (dotted line), momentum distribution $N(p_m)$ (thin solid line), diffusive electric current J (thin dashed line), scattering frequency $\nu(p_m)$ (thin dotted line) and the mean electric field E_0 (thick solid line) on z. The calculations were performed for the normalized shock speed $u_1' = 4900$ km s^{-1}.

u_1', 10^3 km/s[a]	1.55	2.76	4.90	8.25	13.9	23.3	39.2
p_m', TeV/c[b]	9.46	22.7	56.4	120	227	413	854
$<\delta B^2>^{1/2}/B_0$[c]	1.36	4.68	12.6	24.2	44.8	87.3	187
r_b[d]	0.77	0.71	0.77	0.85	0.85	0.84	0.82
$<\delta u^2>^{1/3}/V_a$[e]	5.15	23.6	49.9	94.1	166	361	808
c_s/V_a[f]	1.42	3.70	11.9	31.6	68.4	139	289
$\nu(p_m)/\Omega(p_m)$[g]	1.41	2.63	3.95	4.96	7.21	12.6	22.4
E_0/B_0, 10^{-2}[h]	0.016	0.14	0.74	2.86	10.6	43.7	209
$q\phi/p_m'c$, 10^{-2}[i]	0.348	1.03	2.03	3.30	5.00	7.52	11.0
$D(p_m')/u_1L$, 10^{-2}[k]	9.2	6.8	6.3	6.3	4.9	3.3	2.1
$k_0p_m'c/qB_0$[l]	0.194	1.09	6.15	14.6	34.8	82.7	197

MHD modeling in the shock transition region and downstream of the shock

SW propagation in the medium with density disturbances may also result in magnetic amplification (Giacalone & Jokipii, 2007)

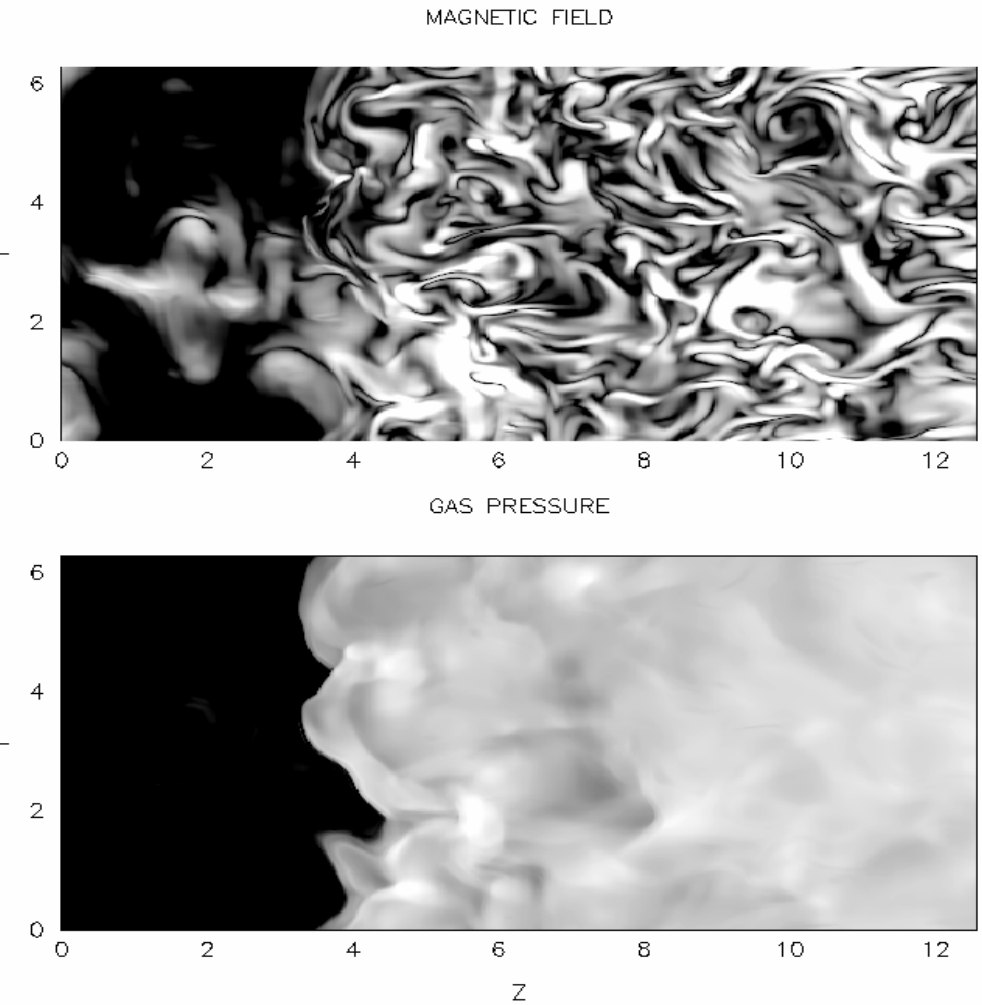

3D $256^2 \times 512$

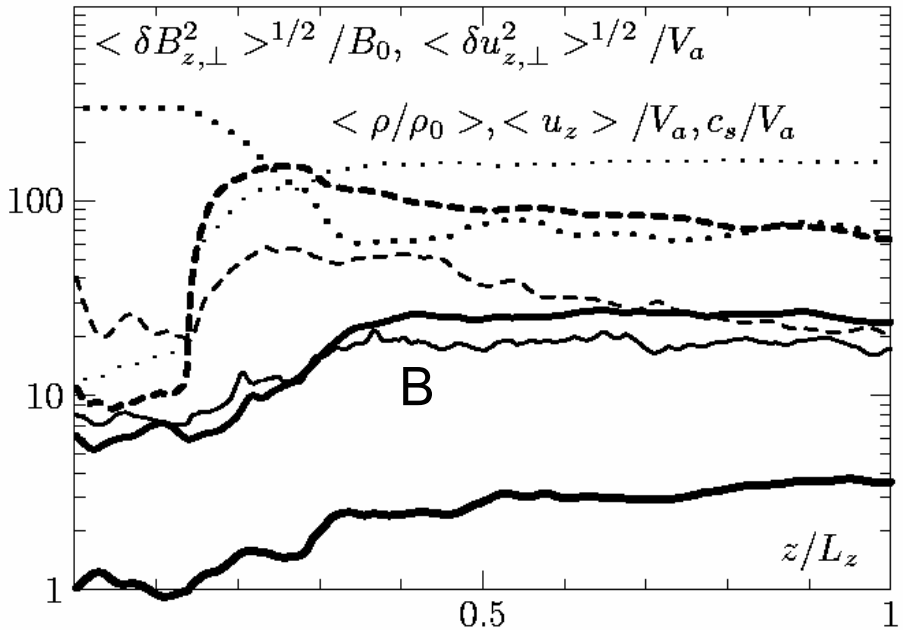

u_1=3000 km/s V_a=10 km/s

u_1'=4900 km/s η_{esc}=0.14

0.02L

Magnetic field is not damped and is perpendicular to the shock front downstream of the shock!

Ratio=1.4 σ_B=3

Schematic picture of the fast shock with accelerated particles

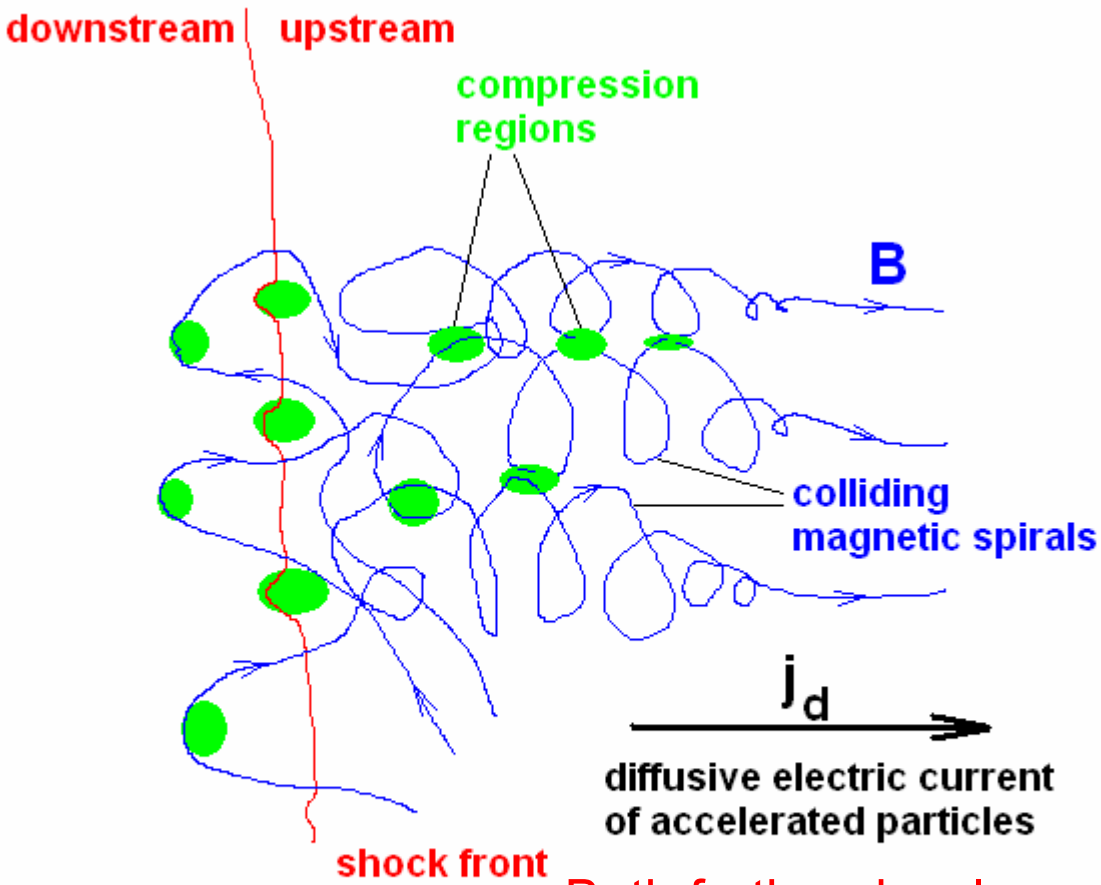

It is a great challenge - to perform the modeling of diffusive shock acceleration in such inhomogeneous and turbulent medium. Spectra of accelerated particles may differ from the spectra in the uniform medium.

Both further development of the DSA theory and the comparison with X-ray and gamma-ray observations are necessary

Wood & Mufson 1992

Dickel et al. 1991

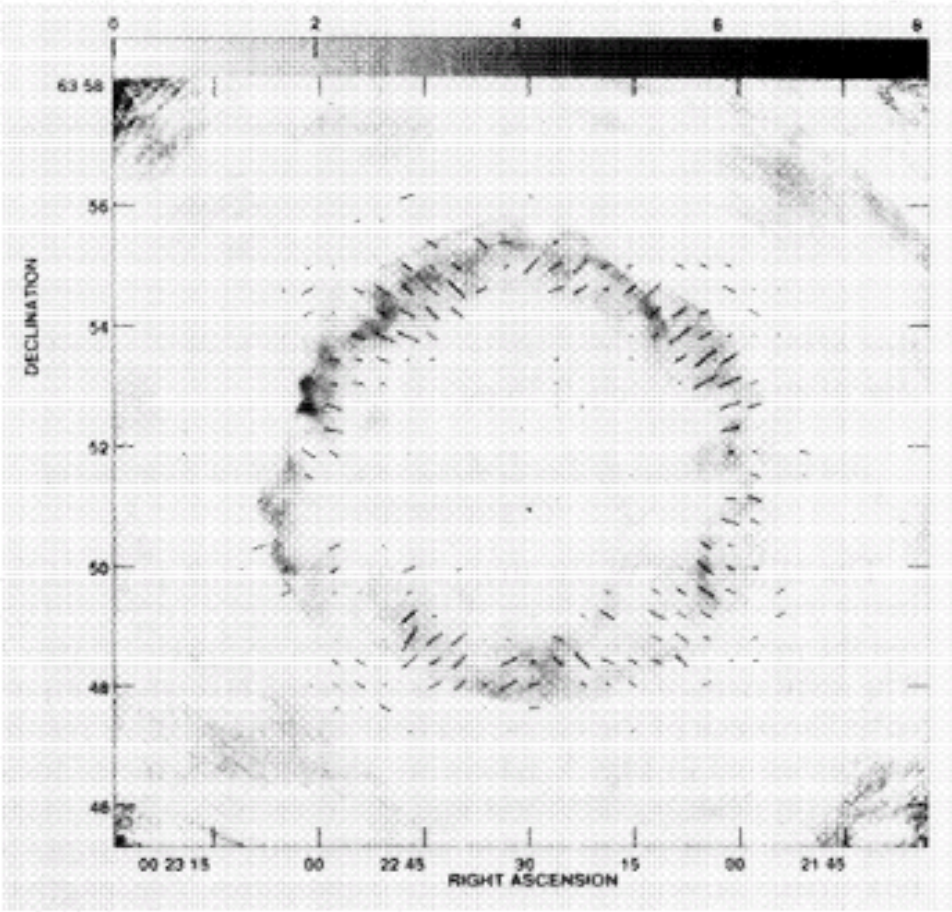

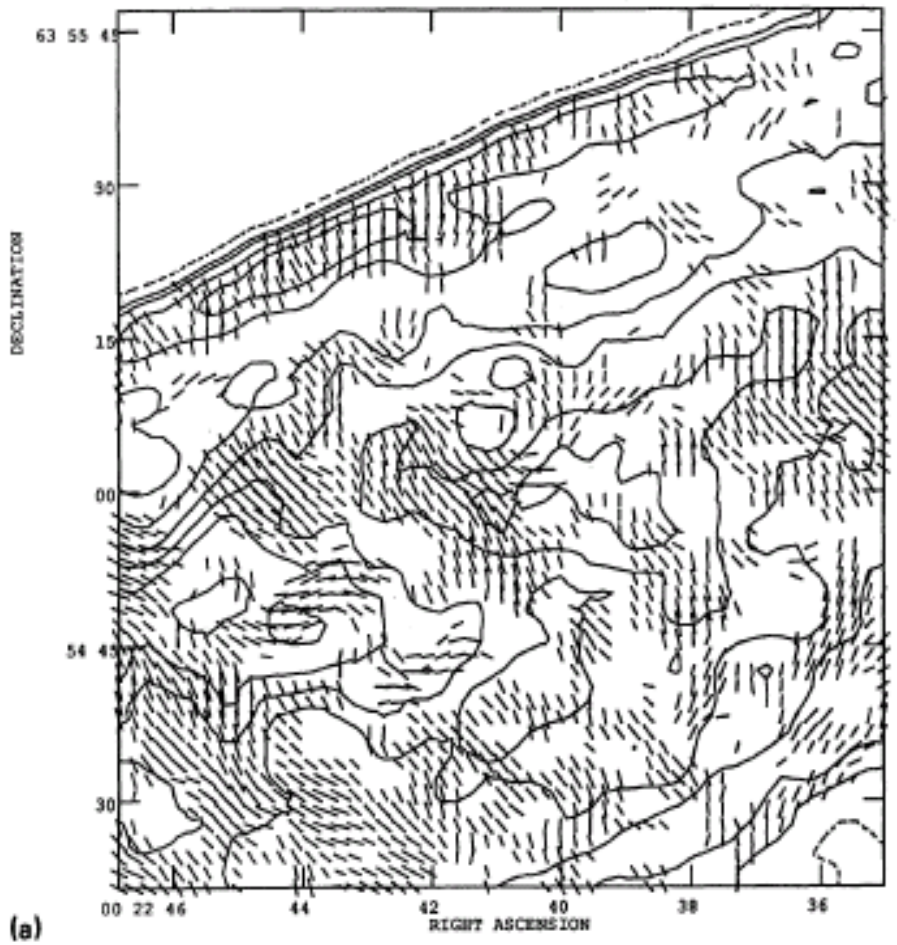

FIG. 5. Map of the remnant of Tycho's supernova showing local magnetic field organization and the direction of the mean local field averaged over boxes of various sizes, superposed on total intensity grey scale as shown in Dickel *et al.* 1991 (Paper I). The length of the vectors indicates the degree of organization in a box, and is proportional to Υ_{org}. The angle of the vector corresponds to the alignment of the mean magnetic field in a box. Positive values of the total intensity are represented with a peak of 8.1×10^{-3} Jy beam^{-1}; the grey scale is in units of 10^{-3} Jy beam^{-1}. (a) Box size of 30×30 pixels (0.55 pc$\times$0.55 pc). (b) Box size of 15×15 pixels (0.27 pc$\times$0.27 pc).

$$B(t) = \begin{cases} B_b \exp(\gamma_{\max} t), \; t < t_1 = \gamma_{\max}^{-1} \ln \frac{2B_0}{B_b} \\ 2B_0(1 + \gamma_{\max}(t - t_1)), \; t > t_1 \end{cases}$$

$$\gamma_{\max} = \frac{\eta_{cr}}{4} \frac{q u_1^3 B_0}{V_a c^2 p_m}. \qquad (35)$$

From these two equations we finally obtain the value of the amplified field

$$B = 2B_0 \begin{cases} u_1^2/u_*^2, \; u_1 < u_* \\ \left(2\frac{u_1^4}{u_*^4} - 1\right)^{1/4}, \; u_1 > u_* \end{cases} \qquad (36)$$

and the maximum energy of accelerated particles

$$p_m c = \frac{\eta_{cr} q u_1^2 B_0 L}{4 c V_a} \begin{cases} \ln^{-1}\left(\frac{2B_0 u_1^2}{B_b u_*^2}\right), u_1 < u_* \\ \left[\ln\left(\frac{2B_0}{B_b}\right) - 1 + \left(2\frac{u_1^4}{u_*^4} - 1\right)^{1/4}\right]^{-1}, \\ u_1 > u_* \end{cases}$$

where the velocity $u_* = (24\pi c V_a^3/\eta_{cr}^2)^{1/4}$.

$$\frac{B^2}{4\pi} \sim 2\eta_{cr}\rho u_1^2 \sqrt{\frac{V_a}{c}}.$$

L=m$_0$R=u$_1$T

Analytical estimate of maximum energies. Max.energy is mainly limited by the finite time of the random magnetic field growth (see also Bell 2004)

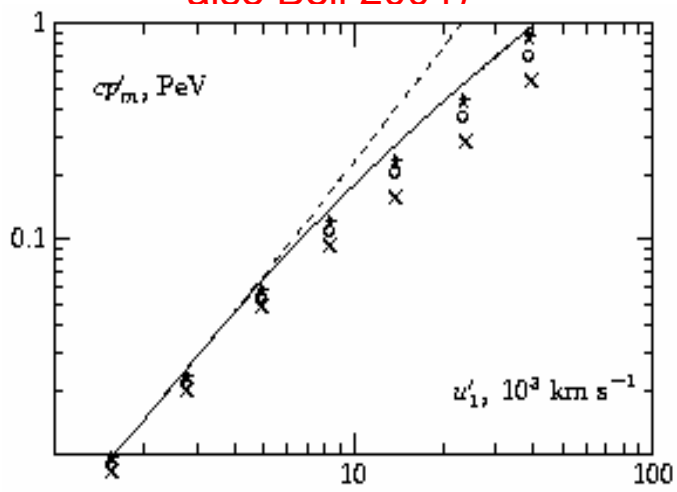

Fig. 5.— The dependence of the normalized maximum momentum p'_m on the normalized shock velocity u'_1. The results were obtained using the resolution 64^3 (crosses), 128^3 (open circles) and 256^3 (stars). The analytic approximation and the upper limit according to Eq. (40) are shown by the solid and dashed lines respectively.

$$\frac{p_m c}{Z} = 21 \text{ TeV} \frac{(\eta_{cr}/0.05)\,(u_1/1000 \text{ km/s})^2\, n_H^{1/2} L_{pc}}{\ln\left(\frac{2B_0}{B_b}\right) - 1 + \left(2\frac{u_1'^4}{u_3^4} - 1\right)^{1/4}} \qquad (39)$$

where Z is the charge number of accelerated particles, $u_3 = 1730$ km/s, n_H is the hydrogen number

Cas A

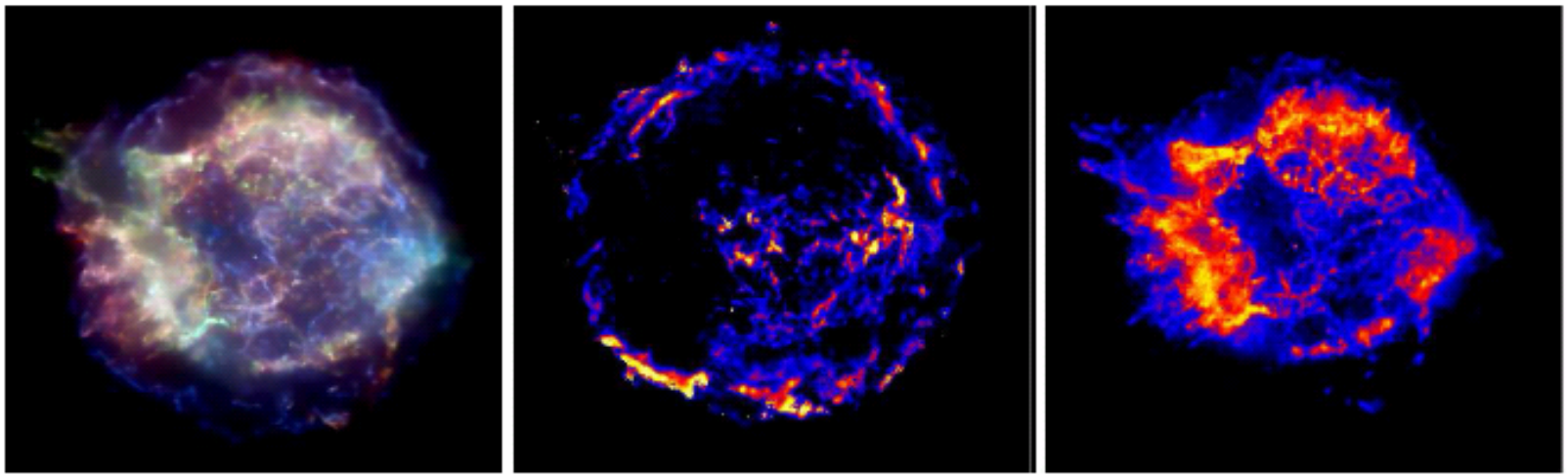

Figure 1. *Left*: A *Chandra* ACIS counts image (log scaling) of Cas A where the red, green and blue colors correspond to the energy bands 0.5–1.5 (i.e. the oxygen, iron, neon and magnesium emission lines), 1.5–2.5 (i.e. the silicon and sulfur emission lines) and 4.0–6.0 keV (i.e. the high-energy continuum), respectively. *Middle*: An image of the fitted bremsstrahlung electron temperature (linear scaling). The values range from about 0.8 keV (blue) to 6.2 keV (yellow). *Right*: An image of the fitted silicon Kα emission line flux (log scaling). The faint, continuum-dominated (i.e. blue-colored) filaments around the outer perimeter of Cas A have relatively hard spectra (i.e. high apparent electron temperatures) and little evidence of line emission.

X-ray imaging of young SNRs with Chandra

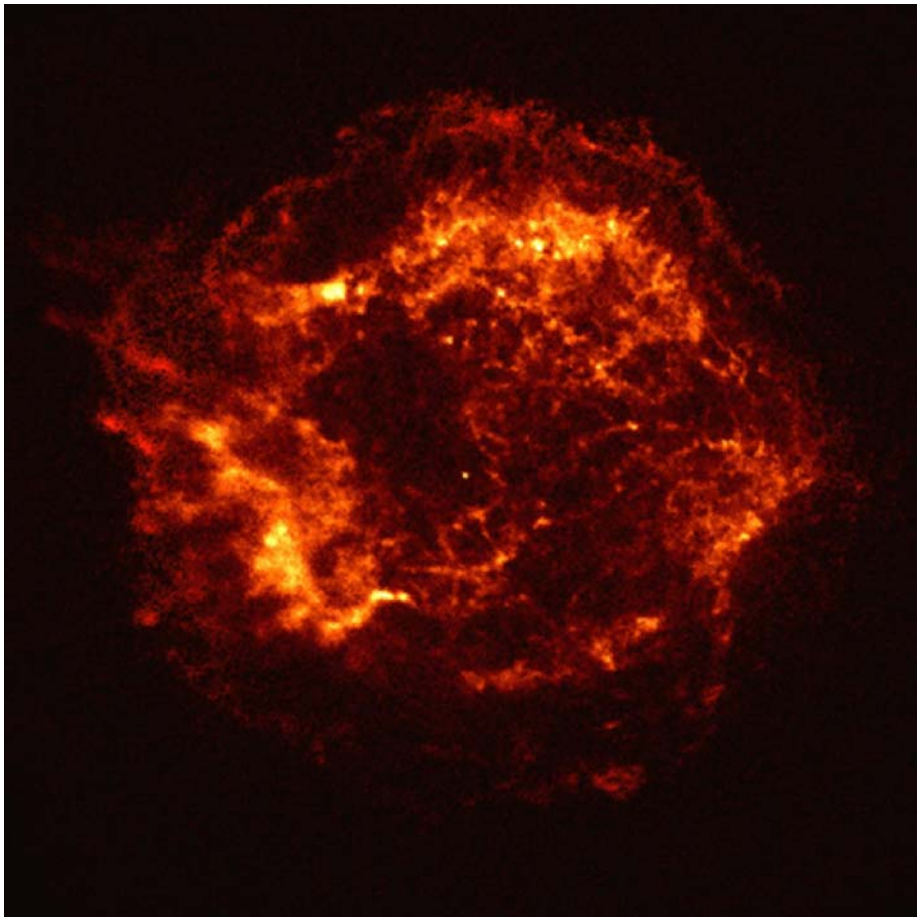

Cas A

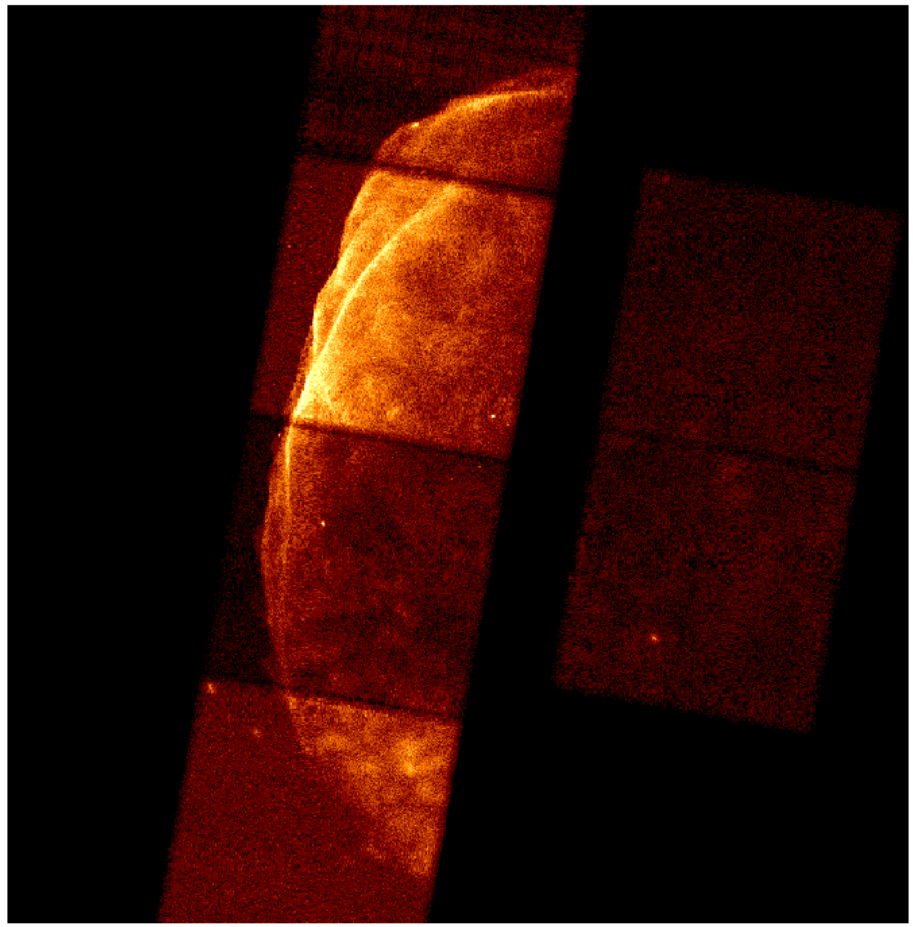

SN 1006

Table 2: Maximum energies and amplified magnetic fields in historical SNRs.

	T^{a}	$u_1{}^{b}$	$n_H{}^{c}$	$B_0{}^{d}$	$u_1'{}^{e}$	$u_1'{}^{e}$	$u_1'{}^{e}$	p_mc^{f}	p_mc^{f}	p_mc^{f}	$B_d{}^{g}$	$B_d{}^{g}$	$B_d{}^{g}$	$B_d^{obs\,h}$
η_{esc}					0.01	0.05	0.14	0.01	0.05	0.14	0.01	0.05	0.14	
Tycho	435	4500	0.3	5.0	1360	3040	5090	19	76	170	21	110	260	300
SN1006	1000	4300	0.1	5.0	860	1920	3220	22	100	240	8.4	43	120	140
Kepler	400	5300	0.35	5.0	1670	3800	6360	30	115	250	33	160	350	215
Cas A	330	5200	3.0	10.0	2220	4960	8300	63	230	500	120	510	980	485

[a] Age of SNR, yr
[b] Forward shock velocity, km s^{-1}
[c] Hydrogen number density of the circumstellar medium, cm^{-3}
[d] Magnetic field strength in the circumstellar medium, μG
[e] Normalized shock velocity, km s^{-1}
[f] Calculated maximum energy p_mc, TeV
[g] Calculated downstream magnetic random field strength, μG
[h] Downstream magnetic field determined from the thickness of X-ray filaments, μG

NOTE.—The numbers from the columns b, c are taken from Vink (2006), the numbers in the last column h are according to Völk et al. (2005)

Max. energy for Cas A was significantly larger in past: 1.2 Z PeV for u_1=10000 km/s

σ_B=4

η_{esc}=0.14: CR modified shock σ=6, σ_s=2.5

η_{esc}=0.01: non-modified shock $P_{CR}=0.1\rho u_1^2$

Rayleigh-Taylor instability of contact discontinuity may also produce amplified radial fields (e.g. Gull 1973)

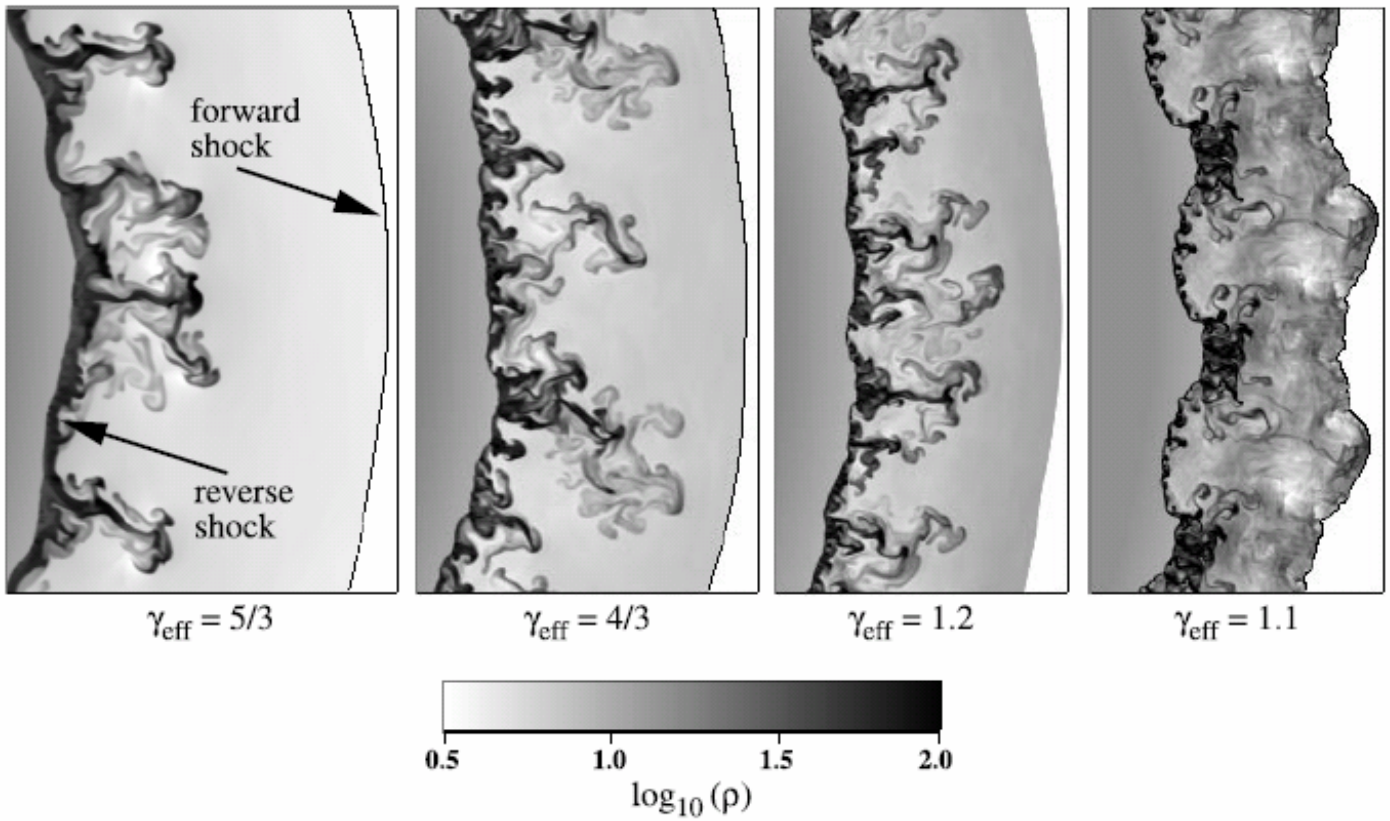

FIG. 4.—Convective instabilities in driven waves with $n = 7$ and $s = 2$ and values of γ_{eff} as marked. The color scale represents gas density, scaled to the density of the CSM immediately ahead of the forward shock. The thin shell of dense, shocked ejecta is deformed into narrow fingers, characteristic of the R-T instability. [*See the electronic edition of the Journal for a color version of this figure.*]

Blondin & Ellison 2001

Magnetic amplification at the shock moving in the nonuniform medium

Inoue et al. 2009

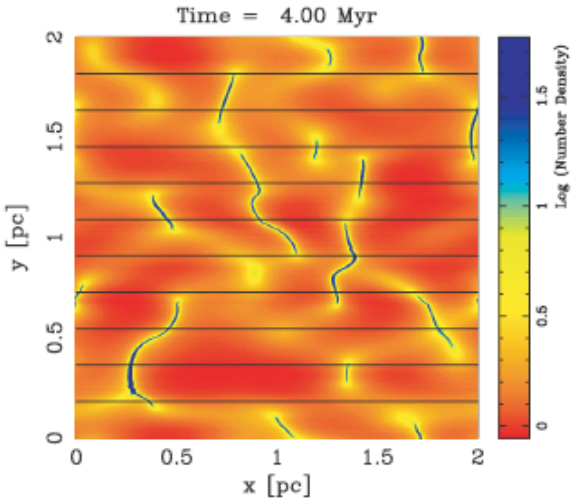

Figure 2. Resulting density structure of Stage 1 at $t = 4.0$ Myr. The black lines show magnetic field lines.

Table 1
Model Parameters

Model	$p_{\rm th}/k_{\rm B}$	Shock Type	Shock Speed
1	3.0×10^8 K cm^{-3}	Perpendicular shock	1256 km s^{-1}
2	3.0×10^8 K cm^{-3}	Parallel shock	1289 km s^{-1}
3	1.0×10^8 K cm^{-3}	Parallel shock	726 km s^{-1}
4	3.0×10^7 K cm^{-3}	Parallel shock	397 km s^{-1}

for a thermal proton is estimated as

$$l_g = 1.5 \times 10^9 \left(\frac{p/k_{\rm B}}{3 \times 10^8 \text{ K cm}^{-3}}\right)^{1/2} \times \left(\frac{n}{10 \text{ cm}^{-3}}\right)^{-1/2} \left(\frac{B}{6\ \mu\text{G}}\right)^{-1} \text{cm}, \quad (6)$$

which is much smaller than the spatial resolution of our numerical simulations and justifies (magneto-)hydrodynamics approximation.

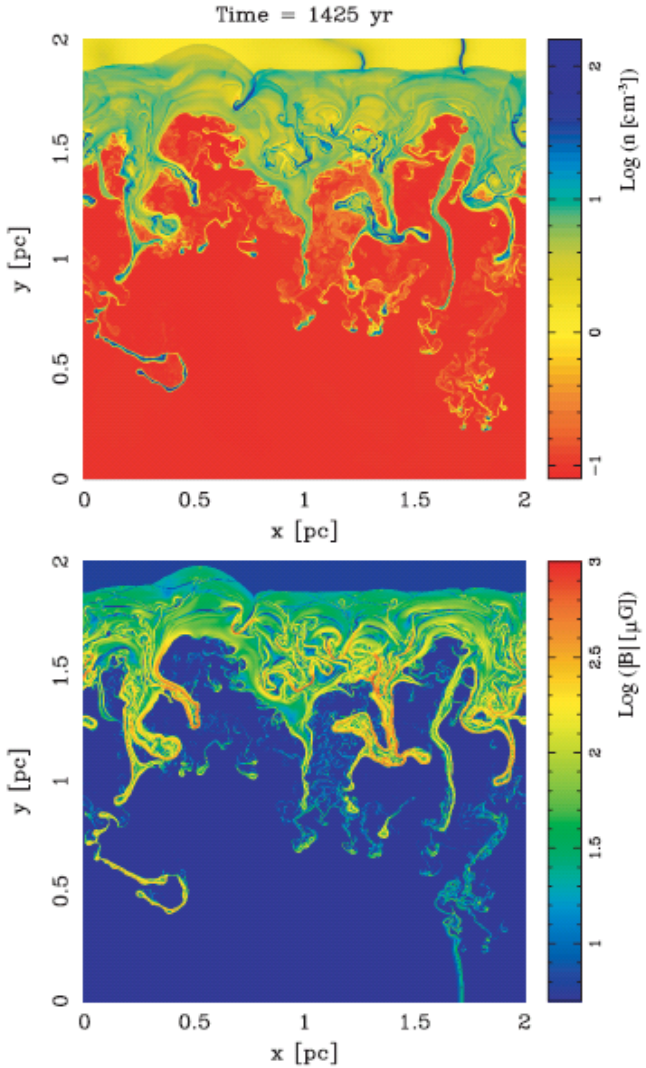

Figure 3. Results of Model 1. The top and bottom panels respectively represent the structure of the number density and magnetic field strength.

Density perturbtions produce vortex motions downstream the shock (Kontorovich 1959, McKenzie & Westphal 1968, Bykov 1982). These motions amplify magnetic fields (Giacalone & Jokipii 2007).

Mean amplification factor ~ 20 for perp. shock even without CRs

Magnetic amplification in the precursor . Shock modification by cosmic ray pressure.

Axford 1977, 1981
Eichler 1984

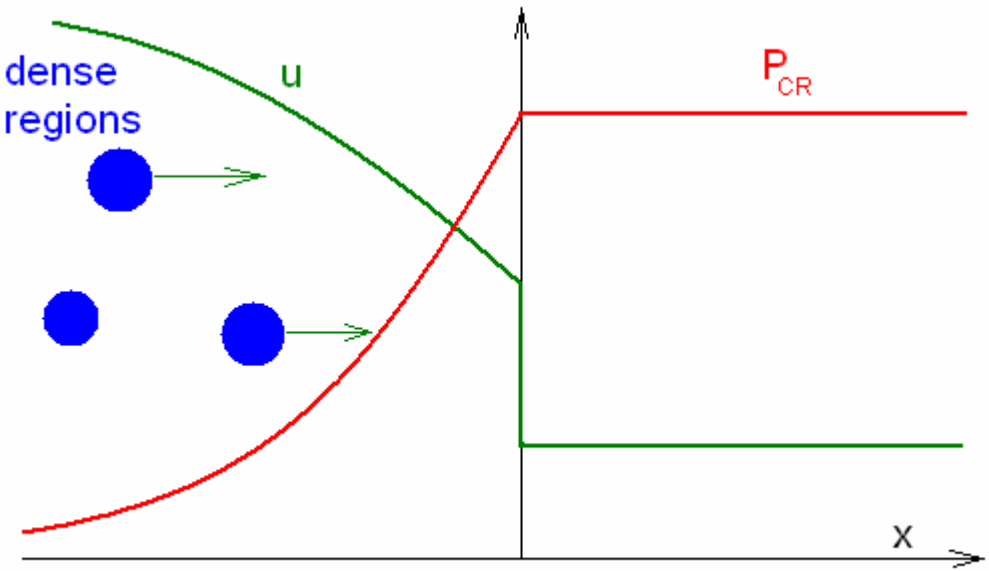

Drury instability.

Discovered by Dorfi (1984) numerically.

Perturbations of the gas density and velocity are amplified. Weak shocks are formed. Heating of the upstream plasma.

If some part of energy goes into the vortex motions, the magnetic field amplification upstream of the shock is possible (Bereznyak et al. 2009)

Summary

1. Non-resonant streaming instability produced by the electric current of run-away CR particles results in the significant magnetic amplification at fast SNR shocks.
2. The perpendicular to the shock front component of the amplified magnetic field is larger than the parallel components downstream of the shock. This naturally explains the preferable radial orientation of magnetic fields in young SNRs.
3. The values of amplified fields are similar to those, observed in historical SNRs, if $\eta_{esc}>0.05$.
4. The maximum energies: 100-300 Z TeV, Ia/b/c and IIP , 1-2 Z PeV for IIb supernovae.
5. Further development of the DSA theory at the corrugated shock (spectra) and the comparison with X-ray and gamma-ray observations are necessary.
6. Another models of the magnetic amplification are possible.